RSC Publishing Faraday Discussions

Ion Reactions in Atmospherically-Relevant Clusters: Mechanisms, Dynamics and Spectroscopic Signatures

Journal:	*Faraday Discussions*
Manuscript ID	FD-ART-12-2018-000230
Article Type:	Paper
Date Submitted by the Author:	05-Dec-2018
Complete List of Authors:	Gerber, Robert; The Hebrew University of Jerusalem , Chemistry; University of California, Irvine, McCaslin, Laura; University of California Irvine Department of Ecology and Evolutionary Biology Karimova, Natalia; University of California, Irvine,

Ion Reactions in Atmospherically-Relevant Clusters: Mechanisms, Dynamics and Spectroscopic Signatures

Natalia V. Karimova[1*], Laura M. McCaslin[2*] and R. Benny Gerber[1,2**]

[1]Department of Chemistry, University of California, Irvine, CA 92697, USA

[2]Institute of Chemistry and Fritz Haber Research Center, Hebrew University of Jerusalem, Jerusalem 91904, Israel

Abstract

Reactions of nitrogen oxides with seawater are of major atmospheric importance, but microscopic understanding of these processes is still largely unavailable. In this paper we explore models of reactions of N_2O_4 with ions in water in order to provide molecular-level understanding into the processes. Presented here are studies of N_2O_4 interacting with two ions, SO_4^{2-} and Cl^-, in small water clusters. Reactions of the asymmetric conformer of N_2O_4 with SO_4^{2-} ions in water clusters are studied via *ab initio* molecular dynamics (AIMD) simulations in order to unravel the microscopic mechanism of the processes and predict the timescales of different steps. Spectroscopic signatures of the reaction are proposed. The mechanisms of chloride substitution and hydrolysis of symmetric and asymmetric N_2O_4 are explored via intrinsic reaction coordinate (IRC) calculations. Spectroscopic calculations for relevant species suggest possible experimental signatures for the processes. The results of these model ion-N_2O_4 reactions in water throw light on the molecular-level mechanisms of the reactions of nitrogen oxides with seawater.

1. Introduction

Nitrogen oxides, including NO_2, NO_3, N_2O_4 and N_2O_5, play key roles in the chemistry of the atmosphere.[1] In addition to gas phase reactions, much of the importance of these molecules is due to heterogeneous processes that several of these species undergo in aqueous environments, including liquid water, aerosols and cloud drops.

One key heterogeneous reaction of nitrogen oxides in the atmosphere is the hydrolysis of N_2O_5 in aqueous aerosols, the main removal process of this molecule from the atmosphere at nighttime that produces the acid HNO_3.[2-5] In addition to hydrolysis, N_2O_5 is known to react with halide-containing salty water, to form XNO_2 (X=Cl, Br, I), which is a source of reactive halogen atoms in the atmosphere.[5-9] The microscopic mechanisms of halide substitution in N_2O_5 have not yet been unraveled, and work on this topic is currently underway.[10] More is presently known on non-reactive interaction between N_2O_5 and water, partly due to recent extensive molecular dynamics simulations.[11]

In this paper, we investigate the molecular-level mechanisms of the reactions between atmospherically relevant anions in water and the nitrogen oxide N_2O_4. Present knowledge on this

topic is very incomplete, and the challenges are similar to those encountered for the N_2O_5 reactions. Theoretically, a major difficulty is that the interaction potentials that govern the reactions are complicated due to strong electrostatic interactions and charge transfer processes, and require description by *ab initio* methods of a suitable level. Furthermore, the actual atmospheric systems are extended, nanosize aerosols at the very least, so models must be introduced that enable computationally feasible calculations while still representing the correct chemical mechanisms.

N_2O_4 has two isomers that are believed to play a role in atmospheric processes.[12-17] Symmetric N_2O_4 is the more stable isomer, but the barrier for conversion into the asymmetric, more active form of the molecule that is written as $ONONO_2$ can be overcome, e.g. on water and other surfaces.[13-18] The possibility of such conversion depends on the specific system and on the temperature, and has not yet been unraveled in detail. We will rely here on the experimental evidence on the formation and chemical activity of asymmetric N_2O_4 on water and ice surfaces in atmospheric conditions.[15-16]

In this paper, we computationally explore the reactions of sulfate ions in water clusters with $ONONO_2$ at the surface, as well as the reactions of chloride with both asymmetric and with symmetric N_2O_4 in the small cluster $(N_2O_4)(Cl^-)(H_2O)$. We additionally explore the hydrolysis of $ONONO_2$ in the presence of Cl^-. Previously reported studies include exploration of the hydrolysis of $ONONO_2$ in small water clusters to produce HONO and HNO_3[19], the reaction of $ONONO_2$ with HCl in the cluster $(ONONO_2)(HCl)(H_2O)$,[20, 21] and the reaction of HCl following collision with $ONONO_2$ absorbed on a slab of water.[22] As will be discussed later, there are close connections between the mechanisms of these processes and the reactions considered here, especially that of the Cl^- ion.

The structure of the paper is as follows: Section 2 presents computational studies of $ONONO_2$ at the surface of the cluster $(SO_4^{2-})(H_2O)_{12}$, yielding the dynamics and the reaction pathways of the processes, unraveling the microscopic mechanisms, and suggesting possible spectroscopic signatures for future experiments. Section 3 explores the reaction pathways of the cluster $(N_2O_4)(Cl^-)(H_2O)$ both for asymmetric $ONONO_2$ and symmetric N_2O_4. Conclusions of the reactions of N_2O_4 with ions in the presence of water, and the connections to reactions of N_2O_5, are brought in Section 4.

2. Reactions of N_2O_4 with $(SO_4^{2-})(H_2O)_{12}$

2.1. System and Methods.

Sulfate ions are some of the most abundant ions present in seawater, making their reactions quite important in the atmosphere. Here we present the highly symmetric and compact $(SO_4^{2-})(H_2O)_{12}$ cluster to model the hydrated ion.[23,24] The structure, shown in Fig. 1a, is computed at the PBE0-D/6-31+G* level of theory.[25-28] All calculations were carried out in the QChem program package.[29]

The shell of 12 water molecules shields the sulfate ion by four strongly bound trimer water rings. We aim to understand whether a reagent such as N_2O_4 can penetrate the water layer and react with the sulfate ion. The structures of the symmetric and the asymmetric isomers, computed at

the same level of theory, are shown in Fig. 1b and 1c, respectively. N_2O_4 is calculated to be 11.0 kcal/mol more stable than $ONONO_2$ at their equilibrium structures shown in Fig. 1. The equilibrium structures of $(N_2O_4)(SO_4^{2-})(H_2O)_{12}$ and $(ONONO_2)(SO_4^{2-})(H_2O)_{12}$ are shown in Fig. 2. The energy difference between the two clusters is only 1.8 kcal/mol, indicating that $ONONO_2$ is significantly stabilized upon clustering with the hydrated sulfate, although the symmetric isomer remains the more stable structure.

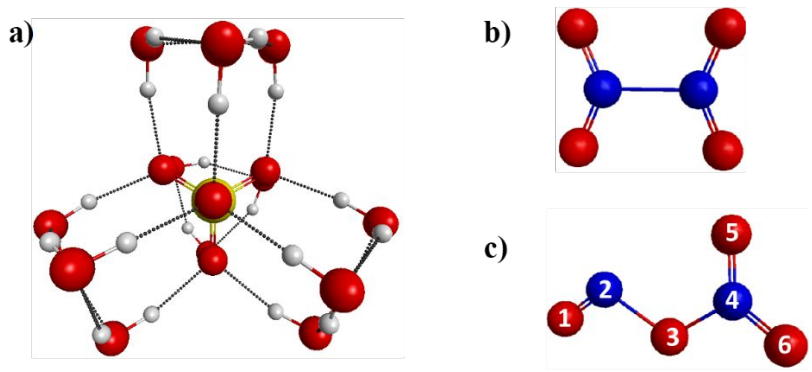

Figure 1 Structures of a) $(SO_4^{2-})(H_2O)_{12}$, b) the symmetric N_2O_4 molecule, and c) the asymmetric *trans*-$ONONO_2$ molecule. Atom colors: red – oxygen, yellow – sulfur, white – hydrogen, and blue – nitrogen.

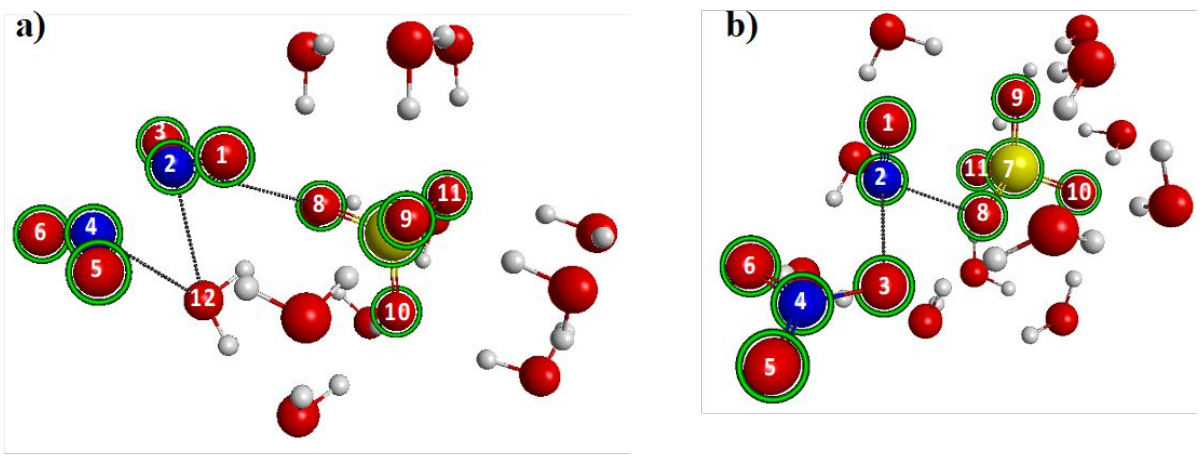

ΔE_{rel} = 0.0 kcal/mol

$R(N_4 \ldots N_2)$ = 1.73 Å $R(N_4 \ldots O_{12})$ = 2.63 Å

$R(N_2 \ldots O_{12})$ = 2.62 Å $R(N_2 \ldots O_8)$ = 3.12 Å

ΔE_{rel} = 1.8 kcal/mol

$R(N_2 \ldots O_3)$ = 2.21 Å

$R(N_2 \ldots O_8)$ = 2.13 Å

Figure 2 Structures, relative energies, and distances in a) $(N_2O_4)(SO_4^{2-})(H_2O)_{12}$, b) $(ONONO_2)(SO_4^{2-})(H_2O)_{12}$. Atom colors: red – oxygen, yellow – sulfur, white – hydrogen, and blue – nitrogen. The atoms of N_2O_4 and SO_4^{2-} are marked by green circles.

The relatively large stabilization of $ONONO_2$ by the water cluster is compatible with experimental evidence, noted previously, that polar $ONONO_2$ is formed and stabilized on ice surfaces due to interactions with free OH groups of amorphous ice.[15,16] Finally, we note that the

binding energy of $ONONO_2$ to the $(SO_4^{2-})(H_2O)_{12}$ cluster, 21.7 kcal/mol, is significantly larger than that of N_2O_4, 12.5 kcal/mol.

To explore the reaction at room temperature between N_2O_4 and the hydrated ion, we used *ab initio* molecular dynamics (AIMD),[30–32] with potentials at the PBE0-D/6-31+G* level of theory. We find that $(ONONO_2)(SO_4^{2-})(H_2O)_{12}$ reacts very quickly while the reaction of $(N_2O_4)(SO_4^{2-})(H_2O)_{12}$ requires much longer timescales. This can be expected due to the relative ease to break the ON–ONO_2 bond compared to the strong N–N bond in N_2O_4. Additionally, the reactions of the asymmetric $ONONO_2$ are sterically favored. It is quite possible that $(N_2O_4)(SO_4^{2-})(H_2O)_{12}$ must first undergo isomerization to the asymmetric isomer before reaction, though the timescales needed to observe such a process are much longer than were studied here. We therefore focus only on clusters containing the asymmetric isomer, $(ONONO_2)(SO_4^{2-})(H_2O)_{12}$, in the dynamics simulations.

2.2. Evolution in Time of Reaction between N_2O_4 and $(SO_4^{2-})(H_2O)_{12}$

Initial velocities were sampled for the equilibrium structure of $(ONONO_2)(SO_4^{2-})(H_2O)_{12}$ from a Boltzmann distribution at room temperature (T = 298 K). A total of 10 reactive trajectories were propagated for up to 7.5 ps using a time-step of 0.4 fs. All the trajectories showed the formation of SO_4NO^- and separation of NO_3^- ion. The product SO_4NO^- was obtained in one of two conformer structures, *cis*-SO_4NO^- and *trans*-SO_4NO^- shown in Fig. 3.

Snapshots of a trajectory leading to *cis*-SO_4NO^- are shown in Fig. 4. Trajectories leading to *trans*-SO_4NO^- are quite similar in character and timescales. In the initial complex $(ONONO_2)(SO_4^{2-})(H_2O)_{12}$ at 0 ps (Fig. 2b, Fig. 4), the $ONONO_2$ molecule is coordinated to the sulfate ion between the $ONONO_2$ terminal nitrogen ($N^{(2)}$) and nearby oxygen ($O^{(8)}$) of the sulfate with distance 2.13 Å (labels given in Fig. 2b). It should be additionally noted that the distance between the NO and NO_3 groups in the $ONONO_2$ molecule increases by 0.67 Å in the presence of the hydrated sulfate ion in comparison to the ON–ONO_2 distance in isolated, gas phase $ONONO_2$.

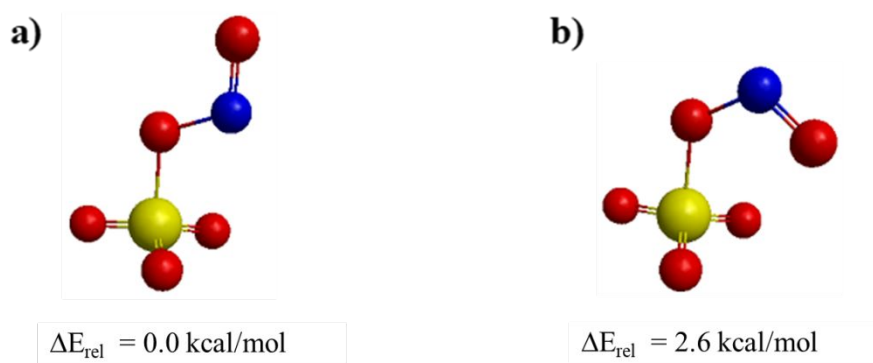

Figure 3 Structures and relative energies of a) *trans*-SO_4NO^- and b) *cis*-SO_4NO^-. Atom colors: red – oxygen, yellow – sulfur, white – hydrogen, and blue – nitrogen.

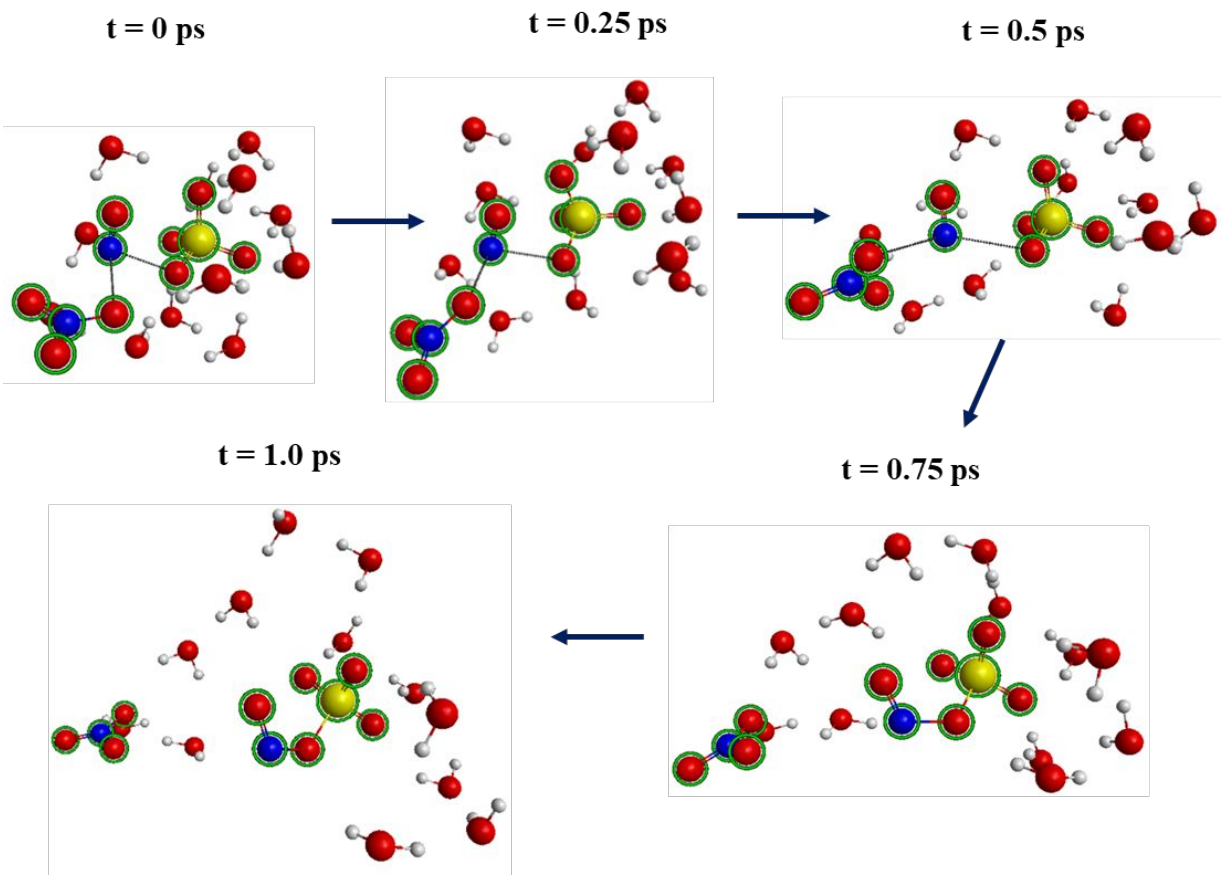

Figure 4 AIMD trajectory configurations with final structure of *cis*-SO_4NO^-. Atom colors: red – oxygen, yellow – sulfur, white – hydrogen, and blue – nitrogen.

In the first 0.5 ps of the process, the distances between the NO and NO_3 groups increase up to 2.65 Å, whereas the distance between the NO and SO_4^{2-} groups remains without significant change at ~ 2.12 Å. In this time, the bond angle $\angle O^{(3)}N^{(2)}O^{(8)}$ increases from 85° to 115° (Fig. 2b). Between 0.5 ps and 0.75 ps, the SO_4NO^- forms via additional shortening of the $O^{(2)}$–$N^{(8)}$ bond distance to 1.76 Å and separation of the NO_3 group, with a $O^{(3)}\ldots N^{(2)}$ coordination distance of 3.41 Å. It should be noted that we considered the average distances and angles for all 10 trajectories at time = 0.5 ps.

In order to consider the changes in partial charge of the SO_4, NO, and NO_3 groups in time, NBO calculations[33] were performed along the trajectories, as shown in Fig. 5 for formation of *cis*-SO_4NO^-. The partial charge of the SO_4 group is seen to decrease from ~ -1.5 a.u. in the initial structure to ~ -1 a.u. after formation of *cis*-SO_4NO^- (Fig. 5a). The positive partial charge on the NO group falls from ~ 0.5 a.u. to ~ 0 a.u. throughout the trajectory. The partial charge on NO_3 group changes very little, from ~ -0.75 a.u. to ~ -1 a.u. (Fig. 5a). Additionally, the evaluation of the charge separation between groups NO^+ and NO_3^- in time is present in Fig. 5b. The results show that initially (from 0 to 0.75 ps), the charge separation between NO and NO_3 moieties is quite substantial (values range from 1.20 – 1.55). After 0.75 ps, this charge separation quickly drops to values around ~1.0, representing the new products. Formation of the SO_4NO^- species is quite fast and occurs due to the attraction of an ion pair (SO_4^{2-}/NO^+) . Overall, the trajectories,

including analysis of the charges, indicate that the reaction occurs from the minimum structure indicated in Fig. 2b within 0.5 to 1.0 ps at 298 K. Inspection of the detailed geometries along the trajectories strongly suggests that the mechanism is of the S_N2 type: as the $ONONO_2$ approaches the SO_4^{2-}, the NO_3^- group is removed from the NO^+ moiety, and a resulting SO_4NO^- species is formed.

The results from these trajectories motivate experimental cluster studies of S_N2-type reactions of $ONONO_2$ in water clusters. Very cold clusters with the structure $(ONONO_2)(SO_4^{2-})(H_2O)_{12}$ can be experimentally isolated. Rapid temperature change to 298K will induce a reaction, such that $ONONO_2$ readily penetrates the water layer around SO_4^{2-}, and an S_N2 type process will take place within 0.5 - 1 ps via charge transfer between the SO_4 and NO groups.

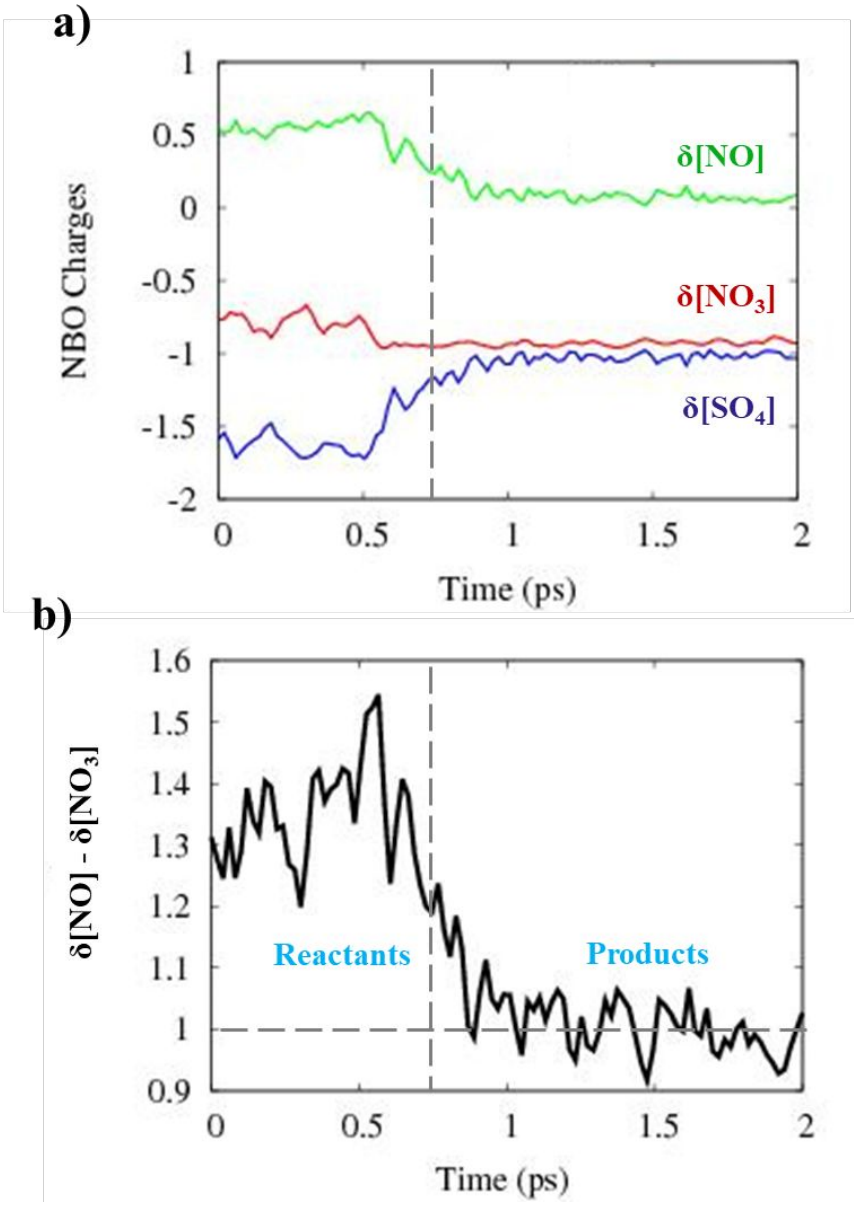

Figure 5 a) Evolution of NBO charges in time along a sample trajectory forming the *cis*-SO_4NO^- product, and b) charge separation between NO^+ and NO_3^- groups.

2.3. IR spectra of *cis/trans*-SO_4NO^-

Infrared (IR) spectroscopy can provide very useful spectroscopic signatures for reaction products and intermediate species for systems including the clusters studied in this work. For instance, the vibrational spectra in the mid-IR range (4000–200 cm^{-1}) may be used to study the fundamental vibrations and associated rotational-vibrational structure.[34,35] One recent and related example is found in the study by P.J. Kelleher et al.[34] on the reactions of N_2O_5 with halide-water clusters, where key intermediates are spectroscopically observed.

In this work, the mid-IR spectrum is simulated for the *cis*- and *trans*- conformers of the SO_4NO^- ion, which may be products or intermediates. A theoretically predicted IR spectrum of the conformers of SO_4NO^- can be useful to experimentalists for detection of this ion in reactions of N_2O_4 and SO_4^{2-} in water. The energy difference between the *cis*- and *trans*- conformers of two forms of SO_4NO^- is 2.6 kcal/mol (Fig. 3). Because both were formed in the dynamical trajectories shown in the previous section, it is important to be able to distinguish the *cis*-SO_4NO^- and *trans*-SO_4NO^- forms in the IR spectra. Additionally, to understand the different contributions of reagent molecules, the vibrational spectra of *trans*-$ONONO_2$ and sulfate ion were calculated. Fig. 6 presents the vibrational spectra of *cis*-SO_4NO^-, *trans*-SO_4NO^-, *trans*-$ONONO_2$ and SO_4^{2-}, with band positions summarized in Tables 1 and 2. Beckers and co-workers[35] showed that the B3LYP[36] functional gives good agreement between theory and experiment for IR spectra of the *trans*-$ONONO_2$ molecule. In this study, the theoretical IR spectra were simulated using the B3LYP method combined with a fairly large basis set 6-311++G**.[27] The IR spectra were calculated for the isolated *trans*-$ONONO_2$ molecule and ions SO_4^{2-} and *cis-/trans*-SO_4NO^- (i.e. no water molecules were included). The B3LYP method was also used to obtain geometrical structures for related isolated species.[37,38] In order to compare the two conformers, we aim to identify and compare IR bands with intensities higher than 100 km/mol.

The IR signals of the *cis*- and *trans*-SO_4NO^- conformers exhibit 15 vibrational modes in the interval 1500 – 900 cm^{-1} (Fig. 6a, 6b and Table 1). Here we will focus on five strong bands in each conformer's spectrum (Fig. 6). The obtained bands I, II, III and V are very similar between the vibrational spectra of *cis*- and *trans*-SO_4NO^-. However, the main difference between their spectra, making them distinguishable, is the intensity and position of band IV (Fig. 6a, 6b and Table 1). This band is a bending mode for the bond angle ∠O–N=O shown in Fig. 3. A band with this character is located at 775.35 cm^{-1} in the case of the *trans*-isomer, whereas for the cis-product, the band is blue-shifted by ~50 cm^{-1}. The differences in intensity and position of IR band IV between the *cis*- and *trans*- isomers can be explained by the steric interaction between the N=O and $–SO_3$ fragments in the *cis*-SO_4NO^- product.

An additional comparison of the IR spectra of the cis- and trans-SO_4NO^- structures with isolated *trans*-$ONONO_2$ and SO_4^{2-} is performed. Band I of the *cis*- and *trans*-SO_4NO^- is the NO stretch of the terminal group (–NO). This same band is observed in the *trans*-$ONONO_2$ but blue-shifted by 300 cm^{-1} (with respect to *cis*-SO_4NO^-) and 280 cm^{-1} (with respect to *trans*-SO_4NO^-) (Fig. 6a, 6c and Table 1, 2). The stretch of the N=O bond in the case of *cis*-SO_4NO^- is ~20% stronger than

obtained for the *trans*-isomer. Band II in the IR spectrum of *cis*- and *trans*-SO_4NO^- is the doubly degenerate asymmetric stretch of the S=O bonds at ~1210 and 1217 cm^{-1} (vibrational modes 2 and 3 in Table 1). This vibrational band is observed in the IR spectrum of isolated sulfate ion at 980 cm^{-1} (Fig. 3d), but the presence of –N=O group shifts this band to the blue by ~240 cm^{-1}. The third strong band (III, mode 5 in Table 1) in the IR signal of the SO_4NO^- ions is a hybrid band. It arises due to a combination of the single N–O bond stretch and symmetric stretch of S=O (Fig. 3, Table 1).

Table 1. Theoretical vibrational frequencies and IR intensities of *cis*-/*trans*-SO_4NO^- at the B3LYP/6-311++G** level of theory.

Mode	***trans*-SO_4NO^-**		***cis*-SO_4NO^-**		Description
	Frequencies, cm^{-1}	**IR intensity, km/mol**	**Frequencies, cm^{-1}**	**IR intensity, km/mol**	
1	1567.44	215.357	1547.9	264.472	$N^{(1)}$=$O^{(2)}$ stretch
2	1219.61	362.303	1213.37	342.627	S=O asym
3	1213.12	344.291	1207.61	309.888	S=O asym
4	1014.97	45.354	975.45	42.73	-
5	938.04	255.065	932.49	262.489	$N^{(2)}O^{(3)}$, S=O sym
6	775.35	250.395	825.68	48.545	$\angle O^{(1)}N^{(2)}O^{(3)}$ bend
7	559.09	446.848	556.15	336.759	SO_3 torsion
8	523.78	29.452	526.78	30.221	-
9	520.75	61.825	495.48	16.951	-
10	374.02	40.84	391.51	0.205	-
11	338.16	0.027	345.41	64.523	-
12	299.36	40.296	281.18	0.962	-
13	210.7	3.025	224.39	0.418	-
14	178.49	3.878	163.9	4.081	-
15	104.14	0.002	116.91	0.002	-

(*) Superscripted numbers denote atom labels shown in Fig. 3.

Table 2. Theoretical and experimental[35] vibrational frequencies and IR intensities of *trans*-$ONONO_2$ at the B3LYP/6-311++G** level of theory.

Mode	**Experiment** [35]	**Theory**		Description
	Frequencies, cm^{-1}	**Frequencies, cm^{-1}**	**IR intensity, km/mol**	
1	1824.9	1848.24	352.946	$N^{(1)}$=$O^{(2)}$ stretch
2	1656.2	1654.94	422.157	NO_2 asym
3	1293.2	1289.67	299.688	NO_2 sym
4	903.3	940.76	30.734	-
5	792.9	807.46	186.169	$\angle O^{(5)}N^{(4)}O^{(6)}$ bend
6	784.1	769.9	32.951	-
7	639	635.9	117.037	$\angle O^{(6)}N^{(4)}O^{(3)}$ bend
8	488.2	489.41	229.82	$N^{(4)}O^{(3)}$ stretch
9	306.0	295.24	315.794	$N^{(2)}O^{(3)}$ stretch
10	-	250.54	1.056	-

11	-	204.31	3.432	-
12	-	92.49	1.154	-

(*) Superscripted numbers denoted the atom labels shown in Fig. 1c.

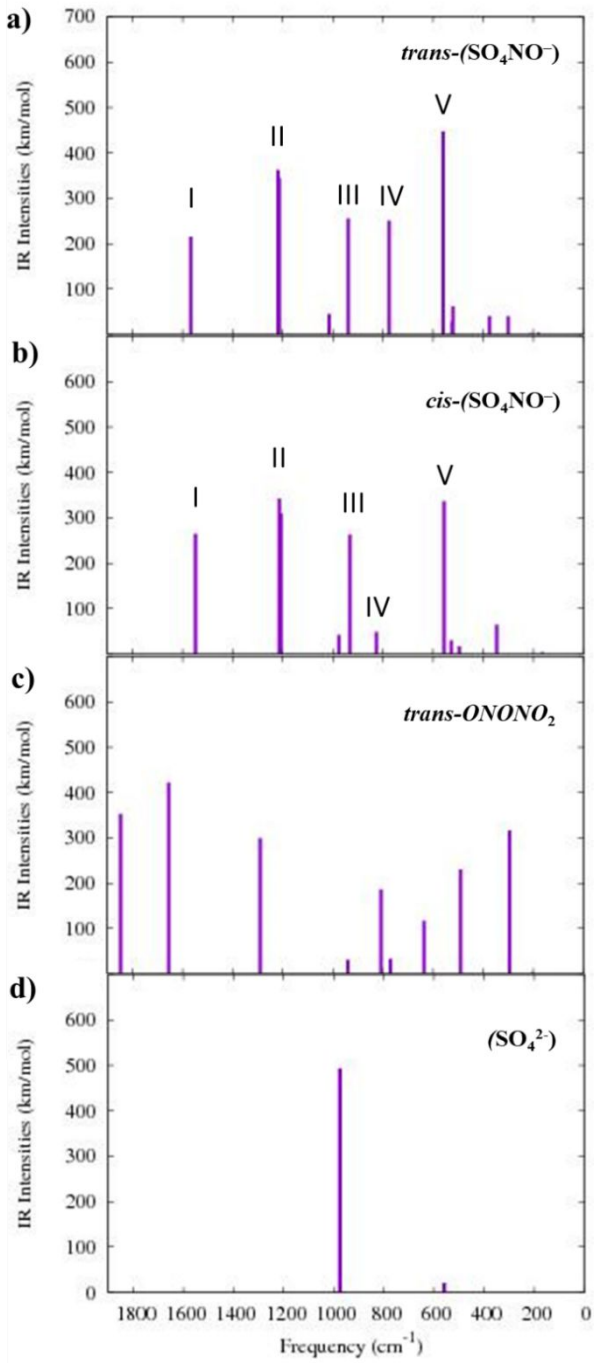

Figure 6 IR spectra of a) *trans*-SO_4NO^-, b) *cis*-SO_4NO^-) c) *trans*-$ONONO_2$, and d) SO_4^{2-} at the B3LYP/6-311++G** level of theory.

3. Reactions of N_2O_4 with $(Cl^-)(H_2O)$

3.1. System and Methods

The reactive mechanisms of $ONONO_2$ with Cl^- in water have been widely debated. Theoretically, small cluster studies of the system $(ONONO_2)(HCl)(H_2O)$ present a minimum structure of $ONONO_2$ electrostatically bound to HCl and H_2O, with a hydrogen bond between the H of HCl and the oxygen of the water. The chlorine atom sits 3.09 A from the nitrogen available for attack.[20,21] The HCl bond must break for transfer of the H to the water, which in turn transfers an H to $NO_3^{\delta+}$ for the Cl to be free to attack the nitrogen, breaking the $ON–ONO_2$ bond, and forming ClNO, H_2O, and NO_3^-. The proton thus plays an integral role in stabilizing the chlorine atom from attacking the nitrogen. Later theoretical studies model a thin film of water with $ONONO_2$ stabilized on the surface.[22] HCl is scattered from the surface of the water, which ionizes quickly. The Cl^- leads the attack on $ONONO_2$, forming ClNO and NO_3^-. This larger model system indicates that the mechanism of chloride substitution of $ONONO_2$ is of the S_N2-type and thus not a proton-led attack. Due to this substantial difference in mechanism between the proton-led attack of the $(ONONO_2)(HCl)(H_2O)$ cluster studies and the S_N2-type substitution of the water slab studies, it is quite desirable to identify model systems that allow one to study the S_N2-type mechanism in detail. Previous cluster studies of the $(ONONO_2)(HCl)(H_2O)$ system will be contrasted with the work here: cluster studies of the negatively charged $(ONONO_2)(Cl^-)(H_2O)$ system. The negatively charged cluster studied here has an additional advantage in that it can be isolated using mass spectrometric techniques.

One major reason that the mechanisms of $ONONO_2$ reactions with Cl^- in water have been so widely debated is lack of clear experimental insights into the atomistic mechanistic details of the processes. In theory, experimental studies of the reactions of $ONONO_2$ in chloride-water clusters could be performed to characterize intermediates of these reactions spectroscopically, as was recently performed by Kelleher et al.[34] It is thus of interest to theoretically identify model cluster systems that contain the key elements for accurately describing atmospherically relevant reactions of $ONONO_2$ in chloride-containing water.

Here we present a study of the small cluster system $(ONONO_2)(Cl^-)(H_2O)$ in order to gain insights into the competition between halide substitution and hydrolysis of asymmetric N_2O_4. We additionally identify barriers and mechanisms for formation of symmetric N_2O_4 from $ONONO_2$. We lastly aim to characterize key intermediates and their spectroscopic signatures for future cluster studies of this system.

In order to characterize reactions of the small cluster system $(ONONO_2)(Cl^-)(H_2O)$, we present intrinsic reaction coordinates (IRC) for key steps in the halide substitution and hydrolysis processes[39]. These were computed at the ωB97X-D/aug-cc-pVDZ level of theory and zero point energy (ZPE) corrected[40,41]. ZPE were calculated in the harmonic approximation. Vibrational frequencies and intensities, also computed in the harmonic approximation, are reported at the same level of theory for key intermediates. This level of theory was used due to its success in previous studies of $(N_2O_5)(Cl^-)(H_2O)$ clusters and related systems[10,34]. All calculations in Section 3 were performed in the QChem program package[29].

3.2. Reaction Pathway of $(N_2O_4)(Cl^-)(H_2O)$

Here we present a study of the reaction pathway of $(N_2O_4)(Cl^-)(H_2O)$ for both symmetric and asymmetric conformers of N_2O_4. It is the aim of this study to compare and contrast the reaction pathways and possible mechanisms between the $(ONONO_2)(Cl^-)(H_2O)$ studied here and previous cluster studies of $(ONONO_2)(HCl)(H_2O)$. Previous studies of the neutral cluster containing HCl indicate that a proton-led attack of $ONONO_2$ prevails. However, HCl is known to rapidly ionize in solution, making a Cl^--led S_N2-type attack more likely in the environment. The present studies of the $(N_2O_4)(Cl^-)(H_2O)$ cluster will allow for detailed information on the microscopic configurations of the cluster for halide substitution and hydrolysis reactions.

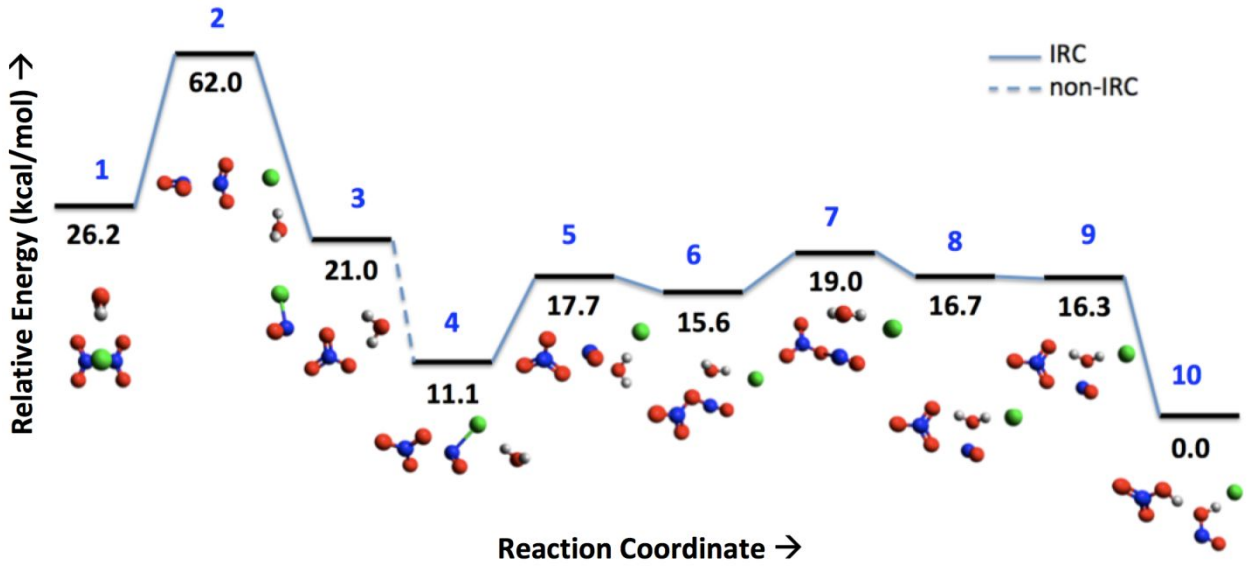

Figure 7 Low-lying reaction pathway of $(N_2O_4)(Cl^-)(H_2O)$. Solid blue lines represent an intrinsic reaction coordinate (IRC), while dotted blue lines do not.

The low-lying reaction pathway for halide substitution and hydrolysis reactions of $N_2O_4 + Cl^- + H_2O$ is shown in Fig. 7. The far left structure with relative energy of 26.2 kcal indicates symmetric N_2O_4 interacting with Cl^-, directly above the N-N bond, and water, forming a hydrogen bond with Cl^-. Section 2 shows that isolated symmetric N_2O_4 is 11.0 kcal/mol more stable than $ONONO_2$. Here it is shown that the low-lying conformer of $(N_2O_4)(Cl^-)(H_2O)$ (1) is 10.6 kcal/mol higher in energy than the minimum structure $(ONONO_2)(Cl^-)(H_2O)$ with relative energy of 15.6 kcal/mol (6). This is quite an interesting result, as it indicates that $ONONO_2$ is highly stabilized by the presence of H_2O and Cl^-. This stabilization of $ONONO_2$ by water and SO_4^{2-} was also observed in Section 2, though the cluster containing symmetric N_2O_4 remained more stable by 1.8 kcal/mol. The chloride substitution reaction of symmetric N_2O_4 has a barrier of 35.8 kcal/mol, indicating that symmetric N_2O_4 requires additional water molecules for this reaction to occur. We therefore focus the majority of our attention on reactions of asymmetric $ONONO_2$ with H_2O and Cl^- in this study.

Two minimum configurations of $(ClNO)(NO_3^-)(H_2O)$ (3 and 4) are shown in Fig. 7, though they are not connected via IRC due to the many complex pathways that connect the structures. Interestingly, the difference in relative energy between the two structures is quite large: 9.9 kcal/mol. The main difference between these configurations is the hydrogen bonding of the

water. In the higher energy configuration, the water forms a hydrogen bond with an oxygen atom on the NO_3^-. Conversely, the lower energy configuration reveals a hydrogen bond between the water and chlorine atom of ClNO. It is clear from the differences in energy that the hydrogen bonding between water and ClNO is very strong and stabilizes this intermediate.

Fig. 7 indicates a minimum geometry of $ONONO_2$ interacting with Cl^- and H_2O at a relative energy of 15.6 kcal/mol (6). On the left of this lies a barrier to chloride substitution of 2.1 kcal/mol. Right of this is a two-step process to hydrolysis. The first step, a barrier of 3.4 kcal/mol indicates formation of a hydrogen bond between the water and an oxygen atom of $ONONO_2$. The pathway continues to a minimum structure at 16.7 kcal/mol (8), revealing the water molecule having two hydrogen bonds: one with the Cl^- and one with the $ONONO_2$. The IRC calculations performed indicate a nearby transition state (at 16.3 kcal/mol) that is lowered in relative energy when the ZPE correction is included. Without the correction, the process is, to numerical accuracy, barrierless. Finally, the hydrolysis product, (HNO_3)(*cis*-HONO)(Cl^-) (10) is found to be the most stable structure in the reaction pathway. Here, the hydrogen atom of HNO_3 makes a hydrogen bond with the adjacent oxygen of *cis*-HONO. The hydrogen atom of *cis*-HONO also makes a hydrogen bond with Cl^-. Both hydrogen bonds greatly stabilize this structure.

3.3. IR Spectra of Key Species in Reactions of $N_2O_4 + Cl^- + H_2O$

In order to make connections between the theoretical reaction pathways described in this section and future experimental studies, we present calculations and analysis of the IR spectra for key species in the processes. The four species with frequencies and intensities presented here are symmetric $(N_2O_4)(Cl^-)(H_2O)$, asymmetric $(ONONO_2)(Cl^-)(H_2O)$, substitution products $(ClNO)(NO_3^-)(H_2O)$, and hydrolysis products $(HNO_3)(HONO)(Cl^-)$, labeled 1, 4, 6, and 10, respectively in Fig. 7. The harmonic frequencies and intensities of these minima, as well as characteristic descriptions for the strongest bands, are given in Tables 3 - 6. The simulated spectra for these clusters are presented in Fig. 8. We aim to identify the key features of the spectra, especially bands that differentiate the four species.

All four species have at least one strong OH stretch, though these bands span over 600 cm^{-1}. The highest energy OH stretch (3648 cm^{-1}) is determined for the $(ClNO)(NO_3^-)(H_2O)$ cluster (4 in Fig. 7). The next highest OH stretch is found at 3568 cm^{-1} in the symmetric $(N_2O_4)(Cl^-)(H_2O)$ cluster (1 in Fig. 7). The asymmetric $(ONONO_2)(Cl^-)(H_2O)$ species (6 in Fig. 7) has a strong OH stretch at 3296 cm^{-1}, while the $(HNO_3)(HONO)(Cl^-)$ cluster (10 in Fig. 7) has a strong OH stretch at 3032 cm^{-1}. All four of these stretches indicate hydrogen stretching toward the chlorine atom, indicating a wide range of hydrogen bonding strengths between these species.

The symmetric $(N_2O_4)(Cl^-)(H_2O)$ species (Table 3 and Fig. 8a) is the most different in structure from the other species studied here. This structure has strong NO stretching bands at 1874 and 1368 cm^{-1}. This species also has a fairly strong water bend at 1674 cm^{-1}, though this is difficult to differentiate from the NO stretching region. The characteristic band in the symmetric $(N_2O_4)(Cl^-)(H_2O)$ structure is a fairly strong ONO bend at 787 cm^{-1}, which is not observed in the other three structures' spectra.

Three of the five strongest bands of the asymmetric $(ONONO_2)(Cl^-)(H_2O)$ species (Table 4 and Fig. 8b) are NO stretches. The band at 2194 cm^{-1} is the terminal NO stretch, decoupled from NO stretches of the NO_3 subspecies. The NO stretches of the NO_3 subspecies are found at 1582 and 1373 cm^{-1}. The decoupled nature of these stretches as well as the large blue shift of the terminal NO stretch indicates that the asymmetric $ONONO_2$ has the character of an ion pair (NO_3^-/NO^+) in this structure. The band at 492 cm^{-1} is a mixed node with character of the free OH wag and stretch between NO and NO_3 subgroups, indicating significant interaction between the subgroups.

The spectrum for the species $(ClNO)(NO_3^-)(H_2O)$, formed as a result of the halide substitution reaction, contains two strong bands that indicate formation of the ClN bond. The NO stretch in the ClNO is found at 2079 cm^{-1}, a 115 cm^{-1} red shift from the terminal NO stretch observed in the $(ONONO_2)(Cl^-)(H_2O)$ cluster. This shift is most likely due to the ClN bond perturbing this stretch more than the NO_3 does in the asymmetric $ONONO_2$ cluster. Secondly, the ClN bond stretch is a fairly strong band at 452 cm^{-1}, characterizing the formation of ClNO. The strong NO bands at 1546 and 1384 cm^{-1} are almost identical in character and frequency as those observed in the $(ONONO_2)(Cl^-)(H_2O)$ cluster, indicating that the NO_3 subgroup behaves similarly in the two systems.

The fourth spectrum represented in Fig. 8d is the cluster resulting from a hydrolysis reaction in $(ONONO_2)(Cl^-)(H_2O)$ to form $(HNO_3)(HONO)(Cl^-)$. The five strongest bands in this spectrum all have mixed character and are quite different from the bands of the $(ONONO_2)(Cl^-)(H_2O)$ and $(ClNO)(NO_3^-)(H_2O)$ clusters. Two mixed modes involving the OH stretch of the HONO and the terminal NO stretch of the HONO are found at 1771 and 1525 cm^{-1}. At 1270 and 1083 cm^{-1}, two strong bands are present that represent in sync wagging motion of the hydrogen atoms, having the character of a water bend. The band at 1083 cm^{-1} is also coupled to the stretching motion of the central NO bond of HONO.

Due to the significant changes in structure between the four species described here, characteristic bands appear in each spectrum. The studies presented in this work aim to guide future spectroscopic investigation of the halide substitution and hydrolysis reactions of symmetric and asymmetric N_2O_4. Future theoretical and experimental studies involving additional water molecules will greatly enhance understanding of how the microscopic configurations of the species affect the reactivity of N_2O_4, stabilization of the asymmetric vs. symmetric forms, and product yields of HONO vs. ClNO. The studies of this small cluster presented here provide detailed microscopic information on the potential energy surface and mechanisms of the hydrolysis and halide substitution processes of $ONONO_2$.

Table 3. Harmonic frequencies (above 200 cm^{-1}) of $(N_2O_4)(Cl^-)(H_2O)$ cluster at the ωB97X-D/aug-cc-pVDZ level of theory

Mode	$(N_2O_4)(Cl^-)(H_2O)$ cluster		Description
	Frequencies, cm^{-1}	IR intensity, km/mol	
1	3935.10	25.248	-
2	3567.88	562.144	OH stretch toward Cl
3	1872.68	651.435	NO stretch

4	1836.36	0.688	-
5	1674.98	188.730	H_2O bend
6	1466.25	55.023	-
7	1368.36	381.788	NO stretch
8	862.26	3.286	-
9	787.01	196.224	NO_2 bend
10	686.99	3.681	-
11	671.20	40.455	-
12	542.89	0.006	-
13	487.17	96.033	-
14	347.87	0.828	-
15	344.04	57.652	-
16	278.38	0.028	-
17	202.60	26.194	-

Table 4. Harmonic frequencies (above 200 cm^{-1}) of $(ONONO_2)(Cl^-)(H_2O)$ cluster at the ωB97X-D/aug-cc-pVDZ level of theory

Mode	$(ONONO_2)(Cl^-)(H_2O)$ cluster		Description
	Frequencies, cm^{-1}	IR intensity, km/mol	
1	3921.44	44.523	-
2	3296.07	837.972	OH stretch toward Cl
3	2194.43	270.317	Terminal NO stretch
4	1621.56	27.007	-
5	1581.67	596.368	NO stretch on NO_3
6	1372.64	619.712	NO stretch on NO_3
7	1097.96	76.654	-
8	840.73	12.564	-
9	734.50	45.648	-
10	720.15	0.579	-
11	492.32	106.525	Mixed: free OH wag + terminal NO stretch
12	419.95	78.811	-
13	382.76	74.435	-
14	346.24	22.322	-
15	244.00	83.225	-
16	227.56	33.241	-

Table 5. Harmonic frequencies (above 200 cm^{-1}) of $(ClNO)(NO_3^-)(H_2O)$ cluster at the ωB97X-D/aug-cc-pVDZ level of theory

Mode	$(ClNO)(NO_3^-)(H_2O)$ cluster		Description
	Frequencies, cm^{-1}	IR intensity, km/mol	
1	3950.87	55.682	-
2	3648.38	645.594	OH stretch between water and Cl

3	2078.80	517.849	NO stretch on ClNO
4	1665.22	90.060	-
5	1545.58	602.341	Asym. NO stretch on NO_3^-
6	1383.64	713.300	Asym. NO stretch on NO_3^-
7	1109.99	35.225	-
8	853.52	9.381	-
9	746.67	25.914	-
10	724.17	1.681	-
11	633.62	75.946	-
12	451.63	295.631	ClN stretch and ClNO bend
13	426.64	18.013	-
14	306.21	54.832	-
15	265.85	27.220	-
16	222.63	187.260	ClN stretch

Table 6. Harmonic frequencies (above 200 cm^{-1}) of $(HNO_3)(HONO)(Cl^-)$ cluster at the ωB97X-D/aug-cc-pVDZ level of theory

Mode	$(HNO_3)(HONO)(Cl^-)$ cluster		Description
	Frequencies, cm^{-1}	IR intensity, km/mol	
1	3031.53	1977.156	Mixed: OH stretch on HNO_3 + OH stretch on HONO
2	1771.41	994.356	Mixed: OH stretch on HONO + terminal NO stretch on HONO
3	1754.20	369.008	-
4	1524.73	1395.559	Mixed: OH stretch on HONO + terminal NO sym. stretch on HONO
5	1471.42	189.612	-
6	1412.16	440.936	-
7	1270.22	2598.159	Mixed: H wag on HONO + H wag on HNO_3
8	1082.93	559.807	Mixed: H wag on HONO + H wag on HNO_3 + central ON stretch on HONO
9	1062.23	73.142	-
10	1036.64	147.098	-
11	951.75	220.485	-
12	823.14	8.826	-
13	755.38	57.965	-
14	714.71	16.536	-
15	657.41	3.811	-
16	350.88	181.787	-

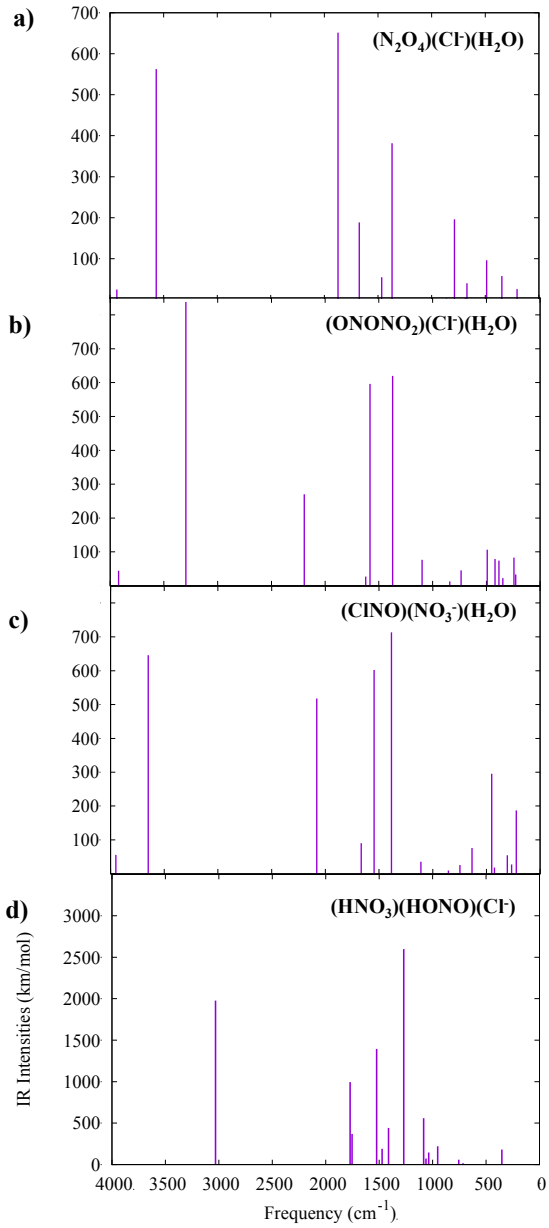

Figure 8 IR spectra of a) symmetric $(N_2O_4)(Cl^-)(H_2O)$, b) asymmetric $(ONONO_2)(Cl^-)(H_2O)$, c) $(ClNO)(NO_3^-)(H_2O)$, and d) $(HNO_3)(HONO)(Cl^-)$ at the ωB97X-D/aug-cc-pVDZ level of theory.

4. Conclusions

This paper explores the reactions of $ONONO_2$ with the ions SO_4^{2-} and Cl^- in water clusters. For both anions, an S_N2-type mechanism involving the terminal nitrogen of the $ONONO_2$ is observed. This suggests that for $ONONO_2$ and related species (including N_2O_5), S_N2-type

substitution reactions are more likely than the electrophilic reactions predicted in previous studies including cluster studies of $(ONONO_2)(HCl)(H_2O)$. The S_N2 reactions of ions with $ONONO_2$ in a water environment described in this work are quite efficient. In a recent study, we also found efficient S_N2 reactions of Cl^- interacting with N_2O_5 and one water molecule. In calculations of IR frequencies and intensities, we identify spectroscopic signatures of key reaction intermediates and products that may be identified in future experiments.

Author contributions

N.V.K. and L.M.M. performed the calculations, provided interpretation of the results, and contributed to the writing of paper. R.B.G. suggested the project, participated in analysis of results, and contributed to the writing of the paper. N.V.K. and L.M.M. made equal contributions to the work as first authors.

Conflicts of interest

There are no conflicts to declare.

Acknowledgements

This research was supported by NSF through the NSF Center for Aerosol Impacts on Chemistry of the Environment (NSF-CAICE), CHE-1801971. Additionally, this work used the Extreme Science and Engineering Discovery Environment (XSEDE),[42] which is supported by National Science Foundation grant number ACI-1548562. L.M.M. would like to thank the Zuckerman STEM Leadership Program for support.

References

1 B.J. Finlayson-Pitts and J.N. Pitts, Jr. "Chemistry of the Upper and Lower Atmosphere", Academic Press, San Diego, 2000.
2 N. Riemer, *J. Geophys. Res*., 2003, 108, 4144.
3 U.F. Platt, A.M. Biermann, R. Atkinson and J.N. Pitts, *Jr. Environ. Sci. Technol*. 1984, 18, 365-369.
4 M. Mozurkewich and J.G. Calvert, *J. Geophys. Res. Atoms*. 1988, 93, 15889-15896.
5 J.A. Thornton and J.P.D. Abbatt, *J. Phys. Chem. A*, 2005, 109, 10004-10012.
6 B.J. Finlayson-Pitts, M.J. Ezell and J.N. Pitts, *Jr. Nature*, 1989, 337, 2412-44.
7 R.C. Hoffmann, M.E. Gebel, B.S. Fox and B.J. Finlayson-Pitts, *Phys. Chem. Chem. Phys*. 2003, 5, 1780-1789.
8 J.A. Thornton, J.P. Korcher, T.P. Riedel, N.L. Wagner, J. Cozic, J.S. Holloway, W.P. Dube, G.M. Wolfe, P.K. Quin, A.M. Middlebrook, B. Alexander and S.S. Brown, *Nature*, 2010, 464, 2712-74.
9 A.D. Hammerich, B.J. Finlayson-Pitts and R.B. Gerber, *Phys. Chem. Chem. Phys*., 2015, 17, 19360-19370.
10 L.M. McCaslin, M.A. Johnson and R.B. Gerber, "Mechanisms and Competition of Halide Substitution and Hydrolysis in Reactions of N_2O_5 with Seawater", (In review).
11 B. Hirshberg, E. Rossich Molina, A.W. Goetz, A.D. Hammerich, G.M. Nathanson, T.H. Bertram, M.A. Johnson and R.B. Gerber, *Phys. Chem. Chem. Phys.*, 2018, 20, 17961-17976.

12 B.J. Finlayson-Pitts, L.M. Wingen, A.L. Summer, D. Syomin and K.A. Ramazan, *Phys. Chem. Chem. Phys.*, 2003, 5, 223.
13 D. de Jesus Medeiros and A.S. Pimentel, *J. Phys. Chem. A*, 2011, 115, 6357-6365.
14 A. Givan and A. Loewenschuss, *J. Chem. Phys*., 1991, 94, 7562.
15 J. Wang and B.E. Koel, *J. Phys. Chem. A,* 1998, 102, 8573.
16 J. Wang and B.E. Koel, *Surf .Sci.*, 1999, 436*,* 15.
17 A.S. Pimentel, F.C.A. Lima and A.B.F. de Silva, *J. Phys. Chem. A*, 2007, 111, 2913.
18 H. Lignell, M.E. Varner, B.J. Finlayson-Pitts and R.B. Gerber, *Chem. Phys*., 2012, 403, 52-59.
19 M.E. Varner, B.J. Finlayson-Pitts and R.B. Gerber, *Phys. Chem. Chem. Phys*., 2014, 16, 4483-4487.
20 J.D. Raff, B. Njegic, W.L. Chang, M.S. Gordon, D. Dabdub, R.B. Gerber and B.J. Finlayson-Pitts, *Proc. Natl. Acad. Sci. (USA)*, 2009, 106, 13647-13654.
21 B. Njegic, J.D. Raff, B.J. Finlayson-Pitts, M.S. Gordon and R.B. Gerber, *J. Phys. Chem. A*, 2010, 114, 4609-4618.
22 A.D. Hammerich, B.J. Finlayson-Pitts and R.B. Gerber, *J. Phys. Chem, Lett*., 2012, 3, 3405-3410.
23 J.C. Hey, L.C. Smeeton, M.T. Oakley, and R.L. Johnston, *J. Phys. Chem. A*, 2016, 120, 4008–4015.
24 L.C. Smeeton, J.D. Farrell, M.T. Oakley, D.J. Wales, and R.L. Johnston, *J. Chem. Theory Comput.*, 2015, 11, 2377–2384.
25 C. Adamo and V. Barone, *J. Chem. Phys*., 1999, 110, 6158.
26 P.M.W. Gill, B.G. Johnson, J.A. Pople and M.J. Frisch, *Chem. Phys. Lett.*, 1992, 197, 499.
27 M.M. Francl, W.J. Petro, W.J. Hehre, J.S. Binkley, M.S. Gordon, D.J. DeFrees and J.A. Pople, *J. Chem. Phys.,* 1982, 77, 3654.
28 S. Grimme, *J. Comput. Chem*., 2006, 27, 1787.
29 Y. Shao, Z. Gan, E. Epifanovsky, A. T. B. Gilbert, M. Wormit, J. Kussmann, A. W. Lange, A. Behn, J. Deng, X. Feng, D. Ghosh, M. Goldey P. R. Horn, L. D. Jacobson, I. Kaliman, R. Z. Khaliullin, T. Kús, A. Landau, J. Liu, E. I. Proynov, Y. M. Rhee, R. M. Richard, M. A. Rohrdanz, R. P. Steele, E. J. Sundstrom, H. L. Woodcock III, P. M. Zimmerman, D. Zuev, B. Albrecht, E. Alguire, B. Austin, G. J. O. Beran, Y. A. Bernard, E. Berquist, K. Brandhorst, K. B. Bravaya, S. T. Brown, D. Casanova, C.-M. Chang, Y. Chen, S. H. Chien, K. D. Closser, D. L. Crittenden, M. Diedenhofen, R. A. DiStasio Jr., H. Dop, A. D. Dutoi, R. G. Edgar, S. Fatehi, L. Fusti-Molnar, A. Ghysels, A. Golubeva-Zadorozhnaya, J. Gomes, M. W. D. Hanson-Heine, P. H. P. Harbach, A. W. Hauser, E. G. Hohenstein, Z. C. Holden, T.-C. Jagau, H. Ji, B. Kaduk, K. Khistyaev, J. Kim, J. Kim, R. A. King, P. Klunzinger, D. Kosenkov, T. Kowalczyk, C. M. Krauter, K. U. Lao, A. Laurent, K. V. Lawler, S. V. Levchenko, C. Y. Lin, F. Liu, E. Livshits, R. C. Lochan, A. Luenser, P. Manohar, S. F. Manzer, S.-P. Mao, N. Mardirossian, A. V. Marenich, S. A. Maurer, N. J. Mayhall, C. M. Oana, R. Olivares-Amaya, D. P. O'Neill, J. A. Parkhill, T. M. Perrine, R. Peverati, P. A. Pieniazek, A. Prociuk, D. R. Rehn, E. Rosta, N. J. Russ, N. Sergueev, S. M. Sharada, S. Sharmaa, D. W. Small, A. Sodt, T. Stein, D. Stück, Y.-C. Su, A. J. W. Thom, T. Tsuchimochi, L. Vogt, O. Vydrov, T. Wang, M. A. Watson, J. Wenzel, A. White, C. F. Williams, V. Vanovschi, S. Yeganeh, S. R. Yost, Z.-Q. You, I. Y. Zhang, X. Zhang, Y. Zhou, B. R. Brooks, G. K. L. Chan, D. M. Chipman, C. J. Cramer, W. A. Goddard III, M. S. Gordon, W. J. Hehre, A. Klamt, H. F. Schaefer III, M. W. Schmidt, C. D. Sherrill, D. G.

Truhlar, A. Warshel, X. Xua, A. Aspuru-Guzik, R. Baer, A. T. Bell, N. A. Besley, J.-D. Chai, A. Dreuw, B. D. Dunietz, T. R. Furlani, S. R. Gwaltney, C.-P. Hsu, Y. Jung, J. Kong, D. S. Lambrecht, W. Liang, C. Ochsenfeld, V. A. Rassolov, L. V. Slipchenko, J. E. Subotnik, T. Van Voorhis, J. M. Herbert, A. I. Krylov, P. M. W. Gill, and M. Head-Gordon, *Mol. Phys.*, 2015, 113, 184–215.

30 D. Matx and J. Hutter, "Ab Initio Molecular Dynamics: Basic Theory and Advanced Methods", Cambridge University Press, New York, 2009.

31 R.B. Gerber, D. Shemesh, M.E. Varner, J. Kalinowski, B. Hirshberg, *Phys. Chem. Chem. Phys.*, 2014, 16, 9760-9775.

32 R.B. Gerber, M.E. Varner, A.D. Hammerich, S. Riikonen, G. Murdachaew, D. Shemesh, B.J. Finlayson-Pitts, *Accts. Chem. Res.*, 2015, 48, 399-406.

33 E. D. Glendening, C. R. Landis, and F. Weinhold, *J. Comput. Chem*., 2013, 34, 1429.

34 P.J. Kelleher, F.S. Menges, J.W. DePalma, J.K. Denton, and M.A. Johnson, G.H. Weddle, B. Hirshberg, R.B. Gerber, *J. Phys. Chem. Lett.*, 2017, 8, 4710–4715.

35 H. Beckers, X. Zeng, and H. Willner, *Chem. Eur. J.*, 2010, 16, 1506-1520.

36 A. D. Becke, *J. Chem. Phys*., 1993, 98, 1372.

37 W.-G. Liu, W.A. Goddard III, *J. Am. Chem. Soc.*, 2012, 134, 12970−12978.

38 R. S. Zhu, K.-Y. Lai, M.C. Lin, *J. Phys. Chem. A*, 2012, 116, 4466−4472.

39 K. Fukui, *J. Phys. Chem.*, 1970, 74, 4161-4163.

40 J.D. Chai and M. Head-Gordon, *Phys. Chem. Chem. Phys.*, 2008, 10, 6610-6615.

41 R.A. Kendall, T.H. Dunning, and R.J Harrison, *J. Chem. Phys.*, 1992, 96, 6796-6806.

42 J. Towns, T. Cockerill, M. Dahan, I. Foster, K. Gaither, A. Grimshaw, V. Hazlewood, S. Lathrop, D. Lifka, G. D. Peterson, R. Roskies, J. R. Scott, N. Wilkins-Diehr, *Comput. Sci. Eng*., 2014, 16, 62-74.